

Gas-Phase Synthesis and Reactivity of the Organomagnesates $[\text{CH}_3\text{MgL}_2]^-$ ($\text{L} = \text{Cl}$ and O_2CCH_3): From Ligand Effects to Catalysis

Richard A. J. O'Hair,* Ana K. Vrkic, and Patrick F. James

Contribution from the School of Chemistry, University of Melbourne, Victoria 3010, Australia

Received March 17, 2004; E-mail: rohair@unimelb.edu.au

Abstract: Multistage mass spectrometry experiments combined with density functional theory (DFT) calculations were used to examine the gas-phase synthesis and ion–molecule reactions of the organomagnesates $[\text{CH}_3\text{MgL}_2]^-$ ($\text{L} = \text{Cl}$ and O_2CCH_3). Neutral species containing an acidic proton (HX) react with the $[\text{CH}_3\text{MgL}_2]^-$ ions via addition with concomitant elimination of methane to form $[\text{XMgL}_2]^-$ ions. Kinetic measurements combined with DFT calculations revealed reduced reactivity of $[\text{CH}_3\text{Mg}(\text{O}_2\text{CCH}_3)_2]^-$ toward water, caused by the bidentate binding mode of acetate, which induces overcrowding of the Mg coordination sphere. The $[\text{CH}_3\text{MgL}_2]^-$ ions reacted with (i) aldehydes with enolizable protons via enolization rather than the Grignard reaction and (ii) $\text{CH}_3\text{CO}_2\text{H}$ to complete a catalytic cycle for the decarboxylation of acetic acid. Other electrophilic reagents such as pivaldehyde, benzaldehyde, methyl iodide, and trimethylborate are unreactive. DFT calculations on the competition between enolization and the Grignard reaction for $[\text{CH}_3\text{MgCl}_2]^-$ ions reacting with acetaldehyde suggest that while the latter has a smaller barrier, it is entropically disfavored.

Introduction

The classic quotes, “no method of organic synthesis superior to that of Grignard’s is known, and indeed there is scarcely any sphere of organic chemistry outside its scope”,¹ “he who knows and understands the Grignard reactions has a fair grasp of organic chemistry”,² and “every organic chemist has carried out the Grignard reaction at least once in their lifetime”,³ highlight the importance of Grignard reagents in organic synthesis.^{4,5} Despite over a century of common use and having been elevated to a top 10 ranking in the most beautiful experiments in chemistry,⁶ their structure (oversimplified as “RMgL” in most undergraduate textbooks), mechanisms of formation, and mode of reactivity (e.g., ionic versus radical) remain topics of lively interest. Deciphering the mechanisms of the reactions of Grignard reagents in solution is complicated by the uncertainty about the nature of the reactive Grignard

species, which can possess various forms existing in equilibrium. These processes include the well-known Schlenk equilibrium (eq 1), dimerization (eq 2), and various ionization modes (eqs 3–5).⁷ Solvation effects add even further complications, since aprotic solvents are typically required to avoid hydrolysis of the Grignard reagent (a simplified reaction with water is shown in eq 6).⁸ Since kinetic studies underpin many mechanistic investigations, the difficulties that these complications present cannot be overstated. In fact, a recent study has cast into doubt an extensive literature accumulated over decades on the kinetics of the classic Grignard reaction, which remains an important reaction used to form carbon–carbon bonds (eq 7).⁹

Several approaches can be adopted to simplify mechanistic studies on organomagnesium systems. The first involves controlling the coordination environment around magnesium to disrupt the Schlenk equilibrium and dimerization. This has been achieved by replacing the traditional halide ligands ($\text{L} = \text{Cl}$, Br , and I) with engineered ligands which can act as multidentate ligands and which can control the steric environment around the magnesium atom. Examples of such ligands include tris-(pyrazoyl)hydroborato ligation, **2**,¹⁰ the use of cryptands and related ligands,¹¹ and the recently developed β -diketiminato

(1) From the presentation speech for Francois Auguste Victor Grignard’s 1912 Nobel prize: <http://www.nobel.se/chemistry/laureates/1912/press.html>.

(2) Kharasch, M. S.; Reinmuth, O. *Grignard Reactions of Nonmetallic Substances*; Prentice Hall: New York, 1954.

(3) Urbanski, T. *Chem. Br.* **1976**, *12*, 191.

(4) For recent monographs and reviews: (a) *Grignard Reagents: New Developments*; Richey, H. G., Jr., Ed.; Wiley: Chichester, 2000. (b) Wakefield, B. J. *Organomagnesium Methods in Organic Synthesis*; Academic Press: London, 1995. (c) *Handbook of Grignard Reagents*; Silverman, G. S., Rakita, P. E., Eds.; Dekker: New York, 1996. (d) Hill, E. A. In *Encyclopedia of Inorganic Chemistry*; King, R. B., Ed.; Wiley: Chichester, 1994; Vol. 1, pp 245–267. (e) Lindsell, W. E. In *Comprehensive Organometallic Chemistry II*; Abel, E. W., Stone, F. G. A., Wilkinson, G., Eds.; Pergamon: Oxford, 1995; Vol. 1, Chapter 3, pp 57–122.

(5) For the sake of simple representation, eqs 1–7 do not include solvent molecules coordinated to magnesium. For an excellent review which brings together a wide range of spectroscopic, physical, and theoretical data to explain the structures of Grignard reagents, see: Ertel, T. S.; Bertagnolli, H. In *Grignard Reagents: New Developments*; Richey, H. G., Jr., Ed.; Wiley: Chichester, 2000; Chapter 10.

(6) Freemantle, M. *Chem Eng News* **2003**, *81* (34), 27.

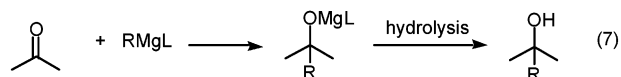
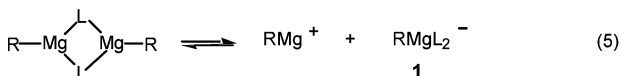
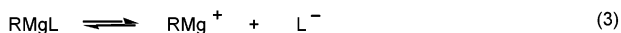
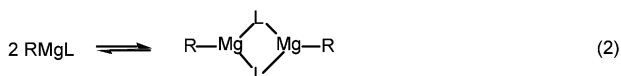
(7) For an excellent review on the Schlenk equilibrium and its effect on reactivity, see: Cannon, K. C.; Krow, G. R. In *Handbook of Grignard Reagents*; Silverman, G. S., Rakita, P. E., Eds.; Dekker: New York, 1996; Chapter 13.

(8) Busch, F. R.; De Antonis, D. M. In *Grignard Reagents: New Developments*; Richey, H. G., Jr., Ed.; Wiley: Chichester, 2000; Chapter 6.

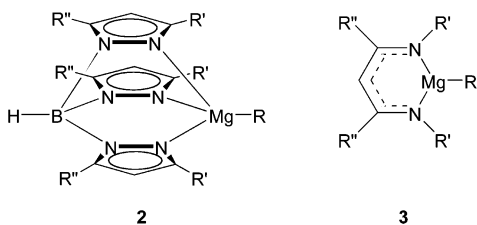
(9) Chubb, J. E.; Richey, H. G. *Organometallics* **2002**, *21*, 3661.

(10) Parkin, G. In *Handbook of Grignard Reagents*; Silverman, G. S., Rakita, P. E., Eds.; Dekker: New York, 1996; Chapter 14.

(11) (a) Tang, H.; Richey, H. G. *Organometallics* **1996**, *15*, 4891. (b) Tang, H.; Parvez, M.; Richey, H. G. *Organometallics* **2000**, *19*, 4810.



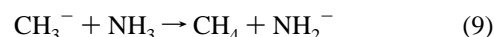
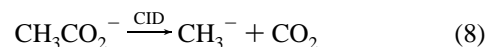
ligands, **3**.¹² Another strategy is to use salt effects to generate



organomagnesate species related to **1**.^{9,13} Alternative approaches include the use of computational chemistry to provide insights into energetics and bonding arrangements of possible species on the potential energy surfaces¹⁴ or the generation and study of solvent-free organomagnesiums.¹⁵

Over the past few decades, gas-phase ion chemistry studies have had a significant impact on our understanding of the fundamental reactivity of a wide range of organic, inorganic, and organometallic species¹⁶ in the absence of solvent, counterions, and clustering interactions. The use of tandem mass

spectrometers in combination with collision-induced dissociation (CID) and ion–molecule reactions (IMR) has proven to be a powerful way of “synthesizing” and studying the bimolecular chemistry of highly reactive species from less reactive precursors. A classic example is Graul and Squires’s synthesis of the bare methyl anion via decarboxylation of the acetate ion (eq 8).¹⁷ The methyl anion is very reactive in the gas phase, even deprotonating weak acids such as ammonia (eq 9).



Electrospray ionization (ESI) has not only revolutionized the analysis of inorganic and organometallic compound via mass spectrometry¹⁸ but also opened up a treasure trove of inorganic ions for fundamental gas-phase chemistry studies. CID of ESI-generated precursor ions has been used to generate a number of novel species. For example, decarboxylation of metal acetates and carbonates can yield organometallics¹⁹ and metal oxo ions.²⁰ Interestingly, these reactions are related to condensed-phase processes. Although the thermal decomposition reactions of metal carboxylates in the condensed phase are quite complex,²¹ there are many examples of the successful application of decarboxylation reactions to the synthesis of organometallics.²² Moreover, the reverse reaction has attracted considerable attention for its relevance to the potential reduction of global greenhouse gas emissions through either carbon dioxide fixation or activation using metal complexes.²³

Here we describe the first gas-phase syntheses of the organomagnesates $[\text{CH}_3\text{MgCl}_2]^-$, **1a**, and $[\text{CH}_3\text{Mg}(\text{O}_2\text{CCH}_3)]^-$, **1b**,²⁴ via decarboxylation of acetate complexes and evaluate their reactivity with neutral reagents such as water and aldehydes using multistage mass spectrometry (MS^n) experiments in a

- (12) (a) Bailey, P. J.; Dick, C. M. E.; Fabre, S.; Parsons, S. *J. Chem. Soc. Dalton Trans.* **2000**, 1655. (b) Bailey, P. J.; Coxall, R. A.; Dick, C. M.; Fabre, S.; Parsons, S. *Organometallics* **2001**, *20*, 798. (c) Dove, A. P.; Gibson, V. C.; Hornmiron, P.; Marshall, E. L.; Segal, J. A.; White, A. J. P.; Williams, D. J. *J. Chem. Soc., Dalton Trans.* **2003**, 3088.
- (13) These charged Grignard reagents are directly relevant to condensed phase studies since they have been implicated in the conductivity of Grignard reagents as well as the enhanced reactivity caused by salt effects. The early literature is summarized in: (a) Loupy, A.; Tchoubar, B. *Salt effects in Organic and Organometallic Chemistry*; VCH: Weinheim, 1992; Chapter 7, pp 250–253. For more recent work, see: (b) Richey, H. G.; DeStephano, J. P. *J. Org. Chem.* **1990**, *55*, 3281. (c) Pajerski, A. D.; Chubb, J. E.; Fabicon, R. M.; Richey, H. G. *J. Org. Chem.* **2000**, *65*, 2231.
- (14) (a) Yamazaki, S.; Yamabe, S. *J. Org. Chem.* **2002**, *67*, 9346. (b) Axten, J.; Troy, J.; Jiang, P.; Trachtman, M.; Bock, C. W. *Struct. Chem.* **1994**, *5*, 99. (c) Oliva, M.; Safont, V. S.; Andrés, J.; Castillo, R.; Moliner, V. *Int. J. Quant. Chem.* **1997**, *65*, 719. (d) Safont, V. S.; Moliner, V.; Oliva, M.; Castillo, R.; Andrés, J.; González, F.; Carda, M. *J. Org. Chem.* **1996**, *61*, 4367. (e) Pérez, E.; Négrel, J.-C.; Goursot, A.; Chanon, M. *Main Group Met. Chem.* **1999**, *22*, 185. (f) Pérez, E.; Négrel, J.-C.; Goursot, A.; Chanon, M. *Main Group Met. Chem.* **1999**, *22*, 201. (g) Ehlers, A. W.; van Klink, G. P. M.; van Eijs, M. J.; Bickelhaupt, F.; Nederkoorn, P. H. J.; Lammertsma, K. *J. Mol. Model.* **2000**, *6*, 186. (h) Sakai, S.; Jordam, K. D. *J. Am. Chem. Soc.* **1982**, *104*, 4019.
- (15) Solvent-free Grignard species have been characterized in the gas phase and in matrix isolation experiments: (a) Himmel, H.-J.; Downs, A. J.; Greene, T. M. *Chem. Rev.* **2002**, *102*, 4191. (b) Imizu, Y.; Klabunde, K. J. *Inorg. Chem.* **1984**, *23*, 3602. (c) Klabunde, K. J.; Whetter, A. *J. Am. Chem. Soc.* **1986**, *108*, 6529. (d) Bare, W. D.; Andrews, L. *J. Am. Chem. Soc.* **1998**, *120*, 7293. (e) Ault, B. S. *J. Am. Chem. Soc.* **1980**, *102*, 10, 3480. (f) Skell, P. S.; Girard, J. E. *J. Am. Chem. Soc.* **1972**, *94*, 5518. (g) Ashby, E. C.; Fernholt, L.; Haaland, A.; Seip, R.; Smith, R. S. *Acta Chem Scand.* **1980**, *34A*, 213.

- (16) (a) Gronert, S. *Chem. Rev.* **2001**, *101*, 329. (b) Fisher, K. J. *Prog. Inorg. Chem.* **2001**, *50*, 343. (c) Schroder, D.; Schwarz, H. *Angew. Chem., Int. Ed. Engl.* **1995**, *34*, 1973. (d) Eller, K.; Schwarz, H. *Chem. Rev.* **1991**, *91*, 1121.
- (17) Graul, S. T.; Squires, R. R. *J. Am. Chem. Soc.* **1989**, *111*, 892.
- (18) For reviews on ESI of inorganic and organometallic species, see: (a) Traeger, J. C. *Int. J. Mass Spectrom.* **2000**, *200*, 387. (b) Colton, R.; D’Agostino, A.; Traeger, J. C. *Mass Spectrom. Rev.* **1995**, *14*, 79. (c) Plattner, D. A. *Int. J. Mass Spectrom.* **2001**, *207*, 125. (d) Gatlin, C. L.; Turecek, F. *Electrospray Ionization of Inorganic and Organometallic Complexes*. In *Electrospray Ionization Mass Spectrometry*; Wiley: New York, 1997; p 527.
- (19) (a) O’Hair, R. A. *J. Chem. Commun.* **2002**, 20. (b) Bachrach, S. M.; Hare, M.; Kass, S. R. *J. Am. Chem. Soc.* **1998**, *120*, 12646.
- (20) Dalgaard, P.; McKenzie, C. J. *J. Mass Spectrom.* **1999**, *34*, 1033.
- (21) Mehrotra, R. C.; Bohra, R. *Metal carboxylates*; Academic Press: London, 1983.
- (22) For a review, see: Deacon, G. B.; Faulks, S. J.; Pain, G. N. *Adv. Organomet. Chem.* **1986**, *25*, 237.
- (23) For recent discussions on the global carbon cycle and the utilization and fixation of CO_2 , see: (a) Arakawa, H.; Aresta, M.; Armor, J. N.; Barteau, M. A.; Beckman, E. J.; Bell, A. T.; Bercaw, J. E.; Creutz, C.; Dinjus, E.; Dixon, D. A.; Domen, K.; DuBois, D. L.; Eckert, J.; Fujita, E.; Gibson, D. H.; Goddard, W. A.; Goodman, D. W.; Keller, J.; Kubas, G. J.; Kung, H. H.; Lyons, J. E.; Manzer, L. E.; Marks, T. J.; Morokuma, K.; Nicholas, K. M.; Periana, R.; Que, L.; Rostrup-Nielson, J.; Sachtler, W. M. H.; Schmidt, L. D.; Sen, A.; Somorjai, G. A.; Stair, P. C.; Stults, B. R.; Tumas, W. *Chem. Rev.* **2001**, *101*, 953. (b) Aresta, M. In *Utilization of Greenhouse Gases*; ACS Symposium Series 852; American Chemical Society: Washington, DC, 2003; p 2. (c) Shi, M.; Shen, Y. M. *Curr. Org. Chem.* **2003**, *7*, 737. For reviews on the activation and coordination chemistry of CO_2 by metal complexes, see: (d) Yin, X. L.; Moss, J. R. *Coord. Chem. Rev.* **1999**, *181*, 27. (e) Leitner, W.; *Coord. Chem. Rev.* **1996**, *153*, 257. (f) Gibson, D. H. *Chem. Rev.* **1996**, *96*, 2063. (g) Braunstein, P.; Matt, D.; Nobel, D. *Chem. Rev.* **1988**, *88*, 747. (h) Behr, A. *Carbon Dioxide Activation by Metal Complexes*; VCH: Weinheim, 1988. (i) Darensbourg, D. J.; Kudarowski, R. A. *Adv. Organomet. Chem.* **1983**, *22*, 129.

Table 1. Summary of Experimental and Theoretical Data for CID Reactions of $[\text{CH}_3\text{CO}_2\text{MgL}_2]^-$

| reaction (eqn no.), $[\text{CH}_3\text{CO}_2\text{MgL}_2]^-$ | branching ratio | threshold (V_{p-p}) and estimate of activation energies (kcal mol ⁻¹) | B3LYP-predicted energetics (kcal mol ⁻¹) | B3LYP-predicted activation energy (kcal mol ⁻¹) |
|---|--------------------|--|---|---|
| 10, L = Cl | | 0.7, 64 | 48.9 | 51.1 |
| 11, L = Cl | | | 78.8 | |
| 10, L = CH_3CO_2 | 0.32 | 0.7, 71 | 47.7 | 54.3 |
| 11, L = CH_3CO_2 | 0.68 | | 51.7 | |

quadrupole ion trap.²⁵ In addition, we use DFT calculations²⁸ to provide further insights into the mechanisms of these reactions.

Experimental Methods

All experiments were carried out using a Finnigan LCQ quadrupole ion trap mass spectrometer modified to allow ion–molecule reactions to be carried out.²⁵ Electrospray solutions were made to 0.1 mg mL⁻¹ in MeOH. Typical ESI conditions: sheath gas flow rate, 60 (arb); auxiliary gas flow rate, 0 (arb); spray voltage, 5 kV; capillary temperature, 150 °C; capillary voltage, -5 V; tube lens offset, -5 V. Multistage mass spectrometry experiments were carried out using the advanced scan function of the LCQ. The ²⁴Mg isotope was mass-selected with a window of 1.5 Th for the ions of interest and subjected to collision-induced dissociation using the following conditions: an activation Q of 0.25, voltage of 0.6, and activation time of 100 ms. Ion–molecule reactions were carried out as previously described.²⁵ Note that in these experiments, the known flow of helium ranged from 1.4×10^5 to 2.2×10^5 mL h⁻¹, while the measured flow of neutral reagent into the helium flow ranged from 0.01 to 0.05 mL h⁻¹. A conservative error in the rate measurements is $\pm 25\%$, but the relative rates are expected to be more accurate due to cancellation of errors. The reaction efficiency is calculated as $\phi = k_{\text{exp}}/k_{\text{ADO}}$, where k_{ADO} is the theoretical prediction of the collision rate²⁶ between $[\text{CH}_3\text{MgL}_2]^-$ (where L = Cl or O_2CCH_3) ion and the neutral reagent.

Using the linear relationship between the threshold activation voltage required for dissociation in ion-trap experiments and the established critical energies for a variety of ions demonstrated by Colorado and Broadbelt²⁷ and by Waters et al.,²⁵ the critical energies of the decarboxylation reactions (eq 10) were roughly estimated. The two species (with known critical energies) that were chosen to “bracket” the activation voltages of the decarboxylation reactions were $\text{Ag}(\text{CH}_3\text{OH})^+$ and $\text{Fe}(\text{C}_5\text{H}_5)_2^+$ (generated via ESI of AgNO_3 in CH_3OH and $\text{Fe}(\text{C}_5\text{H}_5)_2$ in CH_3CN , respectively). Note that the voltages required for the dissociation of these two species that appear in this study were measured by Waters et al.²⁵ It has been previously shown that these species provide useful lower ($\text{Ag}(\text{CH}_3\text{OH})^+$) and upper ($\text{Fe}(\text{C}_5\text{H}_5)_2^+$)

brackets for the activation voltages for several metal ion fragmentation reactions.²⁵ The threshold voltages of the decarboxylation reactions were obtained by (i) mass-selecting a single isotopic peak with an activation time of 10 ms and (ii) increasing the activation voltages (V_{p-p}) until the mass-selected ion was observed to completely dissociate. Following the procedure of Colorado and Broadbelt²⁷ and Waters et al.,²⁵ the “threshold voltage” was defined as the voltage at which the fragment ion intensity was 10% of the total ion intensity.

To gain qualitative insights into the mechanisms of the formation and reactions of the organomagnesates, we have carried out DFT calculations using Gaussian 98²⁸ at the B3LYP level of theory with a 6-31+G* basis set. While an extensive evaluation of the performance of various levels of theory for predicting the structures and energetics of Grignard reactions is lacking,²⁹ we note that the most recent theoretical work on related Grignard reactions used the B3LYP/6-31G* level of theory.^{14a} Given that our systems involve anions, we have also used diffuse functions to help model their structures and energies. Thus, the B3LYP/6-31+G* level of theory is likely to be a reasonable compromise between accuracy and use of computational resources.³⁰ Optimizations were carried out without any symmetry constraints. Vibrational frequency calculations were carried out on each optimized structure at the same level of theory. Reaction energetics were calculated by using the energies listed in the Supporting Information, with the ZPVE corrected by 0.9806.³¹

Results and Discussions

(a) Synthesis via Decarboxylation. Electrospray ionization in the negative ion mode results in magnesium-containing anions of the general formula $[\text{Mg}_n(\text{O}_2\text{CCH}_3)_{2n+1}]^-$ ($n = 1-13$) for magnesium(II) acetate and $[\text{Mg}_n\text{Cl}_i(\text{O}_2\text{CCH}_3)_j]^-$ ($n = 1-3$) for magnesium(II) chloride solution containing acetic acid (data not shown).³² Using the multistage mass spectrometry of our modified quadrupole ion trap, the $[\text{CH}_3\text{CO}_2\text{MgL}_2]^-$ ions can readily be mass-selected to probe their bimolecular and unimolecular chemistry (see Figure S1, Supporting Information). In general, these ions are unreactive toward neutral reagents such as water, methanol, and acetaldehyde (data not shown). The $[\text{CH}_3\text{CO}_2\text{MgL}_2]^-$ ions readily fragment under collisional activation conditions and lead to exclusive decarboxylation when L = Cl (eq 10, Figure S1b) and a combination of decarboxylation (eq 10) and acetate ion formation (eq 11) when L = O_2CCH_3 (Figure S1e). DFT calculations have been carried out on the competing pathways, eqs 10 and 11, for both $[\text{CH}_3\text{CO}_2\text{MgL}_2]^-$ ions (Table 1). They predict that both reactions have similar

(24) There have been two recent reports on the use of mass spectrometry to analyze the composition of Grignard reagents, but their bimolecular gas-phase reactivity has not been experimentally examined: (a) Sakamoto, S.; Imamoto, T.; Yamaguchi, K. *Org. Lett.* **2001**, *3*, 1793. (b) Tjurina, T. A.; Smirnov, V. V.; Barkovskii, G. B.; Nikolaev, E. N.; Esipov, S. E.; Beletskaya, I. P. *Organometallics* **2001**, *20*, 2449.

(25) Waters, T.; O'Hair, R. A. J.; Wedd, A. G. *J. Am. Chem. Soc.* **2003**, *125*, 3384.

(26) Su, T.; Bowers, M. T. *Gas Phase Ion Chemistry*; Academic: New York, 1979; Vol. 1, p 83.

(27) Colorado, A.; Broadbelt, J. *J. Am. Soc. Mass Spectrom.* **1996**, *7*, 1116.

(28) DFT calculations were carried out using: Frisch, M. J.; Trucks, G. W.; Schlegel, H. B.; Scuseria, G. E.; Robb, M. A.; Cheeseman, J. R.; Zakrzewski, V. G.; Montgomery, J. A., Jr.; Stratmann, R. E.; Burant, J. C.; Dapprich, S.; Millam, J. M.; Daniels, A. D.; Kudin, K. N.; Strain, M. C.; Farkas, O.; Tomasi, J.; Barone, V.; Cossi, M.; Cammi, R.; Mennucci, B.; Pomelli, C.; Adamo, C.; Clifford, S.; Ochterski, J.; Petersson, G. A.; Ayala, P. Y.; Cui, Q.; Morokuma, K.; Malick, D. K.; Rabuck, A. D.; Raghavachari, K.; Foresman, J. B.; Cioslowski, J.; Ortiz, J. V.; Baboul, A. G.; Stefanov, B. B.; Liu, G.; Liashenko, A.; Piskorz, P.; Komaromi, I.; Gomperts, R.; Martin, R. L.; Fox, D. J.; Keith, T.; Al-Laham, M. A.; Peng, C. Y.; Nanayakkara, A.; Gonzalez, C.; Challacombe, M.; Gill, P. M. W.; Johnson, B.; Chen, W.; Wong, M. W.; Andres, J. L.; Gonzalez, C.; Head-Gordon, M.; Replogle, E. S.; Pople, J. A. *Gaussian 98*, Revision A.7; Gaussian, Inc.: Pittsburgh, PA, 1998.

(29) Note that work on small inorganic magnesium systems suggests that large basis sets are required to get accurate thermochemistry. See: (a) Petrie, S.; Radom, L. *Int. J. Mass Spectrom.* **1999**, *192*, 173. (b) Alcamí, M.; Gonzalez, A. I.; Mo, O.; Yanez, M. *Chem. Phys. Lett.* **1999**, *307*, 244. (c) Petrie, S. *J. Phys. Chem. A* **2002**, *106*, 5188. (d) Petrie, S. *J. Phys. Chem. A* **2002**, *106*, 7034.

(30) Lynch and Truhlar have noted that the B3LYP/6-31+G** level of theory can yield errors of about 4 kcal mol⁻¹ for the barrier heights for radical reactions: Lynch, B. J.; Truhlar, D. G. *J. Phys. Chem. A* **2001**, *105*, 2936.

(31) Scott, A. P.; Radom, L. *J. Phys. Chem.* **1996**, *100*, 16502.

(32) Related magnesium $[(\text{RCO}_2)_{3-x}\text{MgCl}_x]^-$ anions ions have been reported upon electrospraying mixtures of MgCl_2 and carboxylic acids: Ouyang, S.; Vairavamurthy, M. A. *Anal. Chim. Acta* **2000**, *422*, 101.

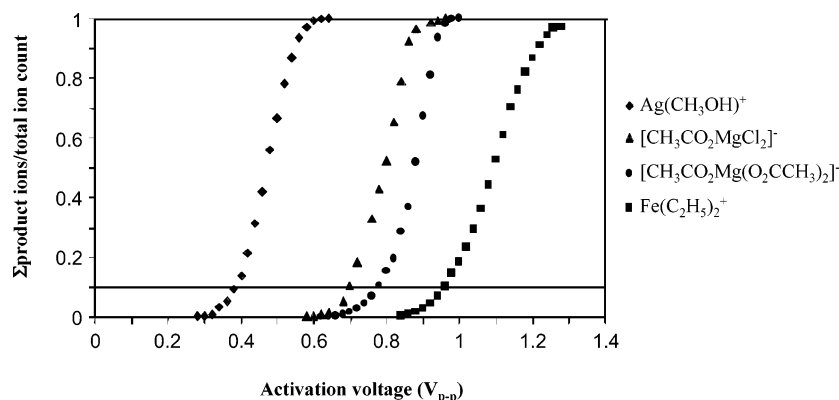
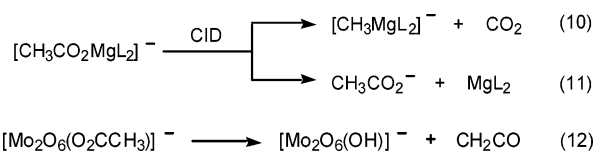


Figure 1. Plot of reaction extent (Σ product ions/total ion count) vs activation voltage (V_{p-p}) for elimination of CO_2 from $[\text{CH}_3\text{CO}_2\text{MgCl}_2]^-$ and $[\text{CH}_3\text{CO}_2\text{Mg}(\text{O}_2\text{CCH}_3)_2]^-$. The critical energies for dissociation of $\text{Ag}(\text{CH}_3\text{OH})^+$ ($33.0 \pm 3.7 \text{ kcal mol}^{-1}$) and $\text{Fe}(\text{C}_2\text{H}_5)_2^+$ ($85 \pm 7 \text{ kcal mol}^{-1}$) are known, and the activation voltage data are taken from ref 25. The line corresponds to 10% reaction extent, the point at which threshold activation voltages are measured.

endoothermicities for $[\text{CH}_3\text{CO}_2\text{Mg}(\text{O}_2\text{CCH}_3)_2]^-$ ($47.7 \text{ kcal mol}^{-1}$ for eq 10 and $51.7 \text{ kcal mol}^{-1}$ for eq 11), but that acetate loss (eq 11) is considerably more endothermic ($78.8 \text{ kcal mol}^{-1}$) than decarboxylation ($48.9 \text{ kcal mol}^{-1}$ for eq 10) for $[\text{CH}_3\text{CO}_2\text{MgCl}_2]^-$. The competition between decarboxylation and acetate ion formation has also been observed for the silver acetate ion, $[\text{Ag}(\text{O}_2\text{CCH}_3)_2]^-$.^{19a} An alternative fragmentation channel of a metal-bound acetate ligand, involving expulsion of ketene and observed for metal oxo ions (eq 12),³³ does not occur.³⁴ Note that collisional activation of the higher clusters of $[\text{Mg}(\text{O}_2\text{CCH}_3)_{2n+1}]^-$ and $[\text{Mg}_n\text{Cl}_x(\text{O}_2\text{CCH}_3)_y]^-$ does not result in loss of CO_2 .



To provide a qualitative insight into the critical energies of these decarboxylation reactions, we have compared the activation voltages required for these reactions with those required for the dissociation of two species with established critical energies, $\text{Ag}(\text{CH}_3\text{OH})^+$ and $\text{Fe}(\text{C}_2\text{H}_5)_2^+$.²⁵ Examination of Figure 1 reveals the following critical energies for dissociation: (i) $33 \pm 3.7 \text{ kcal mol}^{-1}$ (threshold voltage = $0.38 V_{p-p}$) for $\text{Ag}(\text{CH}_3\text{OH})^+$; (ii) $85 \pm 7 \text{ kcal mol}^{-1}$ (threshold voltage = $0.93 V_{p-p}$) for $\text{Fe}(\text{C}_2\text{H}_5)_2^+$; (iii) $0.7 V_{p-p}$ for $[\text{CH}_3\text{CO}_2\text{MgCl}_2]^-$ (eq 10); and (iv) $0.78 V_{p-p}$ for $[\text{CH}_3\text{CO}_2\text{Mg}(\text{O}_2\text{CCH}_3)_2]^-$ (eq

10). This suggests crude estimates of 64 ± 20 and $71 \pm 20 \text{ kcal mol}^{-1}$ for the critical energy of CO_2 elimination from $[\text{CH}_3\text{CO}_2\text{MgCl}_2]^-$ and $[\text{CH}_3\text{CO}_2\text{Mg}(\text{O}_2\text{CCH}_3)_2]^-$, respectively.

To quantitate the competition between decarboxylation and acetate ion formation for $[\text{Mg}(\text{O}_2\text{CCH}_3)_3]^-$, the relative branching ratios of these two channels were examined as a function of the activation amplitude (Figure S2, Supporting Information). When low activation amplitudes were used (i.e., 0.6 V), $[\text{CH}_3\text{CO}_2]^-$ formation was more dominant than $[\text{CH}_3\text{Mg}(\text{O}_2\text{CCH}_3)_2]^-$ formation (i.e., branching ratio $\sim 0.68:0.32$, respectively, Table 1). As the activation amplitude is increased, $[\text{CH}_3\text{CO}_2]^-$ formation still predominates over $[\text{CH}_3\text{Mg}(\text{O}_2\text{CCH}_3)_2]^-$; however, the branching ratios level out to $\sim 0.55:0.45$, respectively.

To gain further insight into the formation of the novel organomagnesates **1a** and **1b**, we carried out DFT calculations on the reaction coordinates associated with decarboxylation (Figure 2) at the B3LYP/6-31+G* level of theory. All of the structures and energies of the species calculated for the decarboxylation reactions are listed in the Supporting Information (Figure S3 and Tables S1 and S2). IRC calculations were carried out in both directions in order to link the transition states to the reactant and products. These IRC calculations revealed a different “reactant” geometry relative to the global minima for $[\text{Mg}(\text{O}_2\text{CCH}_3)_3]^-$ (Figure 2b), but not for $[\text{CH}_3\text{CO}_2\text{MgCl}_2]^-$ (Figure 2a). Figure S3 shows the structures of the key magnesium species associated with decarboxylation: (i) the global minima for the $[\text{CH}_3\text{CO}_2\text{MgL}_2]^-$ reactant ions; (ii) the transition states for CO_2 loss for $[\text{CH}_3\text{CO}_2\text{MgL}_2]^-$; (iii) the $[\text{CH}_3\text{MgL}_2]^-$ product ion structure (when $L = \text{Cl}$ and O_2CCH_3); (iv) the product organomagnesates, **1a** and **1b**; and (v) the “reactive conformation” for the $[\text{CH}_3\text{CO}_2\text{Mg}(\text{O}_2\text{CCH}_3)_2]^-$ species. Figure 2 illustrates the reaction coordinates for the decarboxylation of (i) $[\text{CH}_3\text{CO}_2\text{MgCl}_2]^-$ and (ii) $[\text{Mg}(\text{O}_2\text{CCH}_3)_3]^-$. An examination of the transition states reveals that these decarboxylation reactions share the similar features of a four-centered transition state where the CH_3 group transfers from the carboxyl moiety to the electrophilic MgL_2 center, ultimately yielding carbon dioxide and the organomagnesates **1a** and **1b**. $[\text{CH}_3\text{CO}_2\text{Mg}(\text{O}_2\text{CCH}_3)_2]^-$ is predicted to have a higher activation barrier than $[\text{CH}_3\text{CO}_2\text{MgCl}_2]^-$, which is entirely consistent with the experimentally determined thresholds

(33) Waters, T.; O'Hair, R. A. J.; Wedd, A. G. *Int. J. Mass Spectrom.* **2003**, *228*, 599.

(34) It is interesting to compare the fragmentation behavior of metal carboxylates (eqs 10–12) to the decomposition of acetic acid, which yields two sets of reaction products formed under thermal conditions: (i) ketene and water, and (ii) methane and carbon dioxide. Thus, (i) the ketene channel is related to that observed for metal oxo anions (eq 12), and (ii) the decarboxylation channel is relevant to the formation of the organomagnesates (eq 10). Activation energies for these reactions are as follows: (i) for the ketene channel, experiment $65\text{--}73 \text{ kcal mol}^{-1}$,^{34a–d} and theory $72\text{--}76 \text{ kcal mol}^{-1}$,^{34e,f} and (ii) for the decarboxylation channel, experiment $60\text{--}73 \text{ kcal mol}^{-1}$,^{34a–d} and theory $67\text{--}72 \text{ kcal mol}^{-1}$,^{34e,f}. Note that decarboxylation not only has a slightly lower activation energy than that predicted for dehydration, but it is favored on thermodynamic grounds by over 40 kcal mol^{-1} . For key references see: (a) Bamford, C. H.; Dewar, M. J. S. *J. Chem. Soc.* **1949**, 2877. (b) Blake, P. G.; Jackson, G. E. *J. Chem. Soc., B* **1969**, *1*, 94. (c) Mackie, J. C.; Doolan, K. R. *Int. J. Chem. Kinet.* **1984**, *16*, 525. (d) Butkovskaya, N. I.; Manke, G., II; Setser, D. W. *J. Phys. Chem.* **1995**, *99*, 11115. (e) Fang, W.-H.; Liu, R.-Z.; Zheng, X.; Phillips, D. L. *J. Org. Chem.* **2002**, *67*, 8407. (f) Takahashi, O.; Itoh, K.; Saito, K. *Theochem* **2002**, *584*, 249.

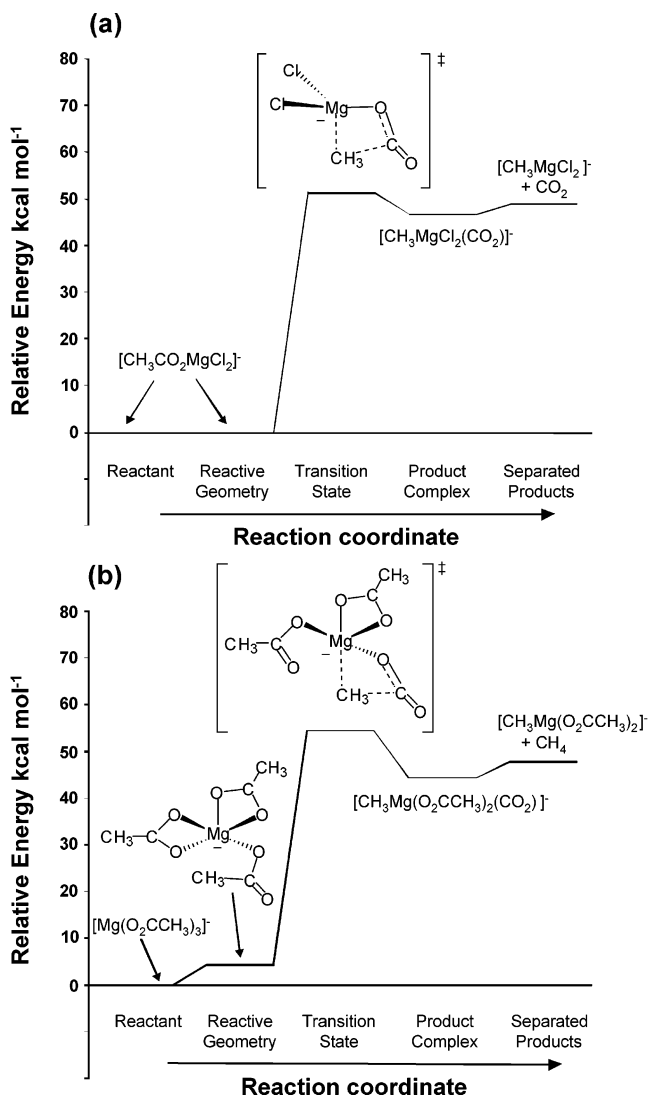


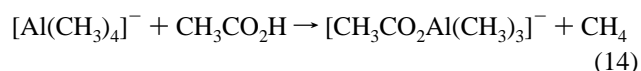
Figure 2. Plot of B3LYP/6-31+G*-calculated reaction coordinate for CO₂ loss from (a) [CH₃CO₂MgCl₂]⁻ and (b) [Mg(O₂CCH₃)₃]⁻.

(Figure 1). Table 1 summarizes the key experimental and theoretical data associated with reactions 10 and 11 for both systems.

Finally, a comparison of the DFT-optimized structures of the two organomagnesates [CH₃MgL₂]⁻ (Figure S3) reveals some interesting structural features relating to the bonding arrangements of the ancillary ligands, L. [CH₃MgCl₂]⁻ (**1a**) is predicted to have a three-coordinate trigonal planar structural with a CH₃–Mg bond length of 2.137 Å and Mg–Cl bond lengths of 2.338 Å. In contrast, [CH₃Mg(O₂CCH₃)₂]⁻ (**1b**) is predicted to have a five-coordinate structure with a CH₃–Mg bond length of 2.158 Å and bidentate acetate ligands with nonequivalent Mg–O bond lengths (of about 2.14 and 2.23 Å). While it is not possible to make direct comparisons with X-ray crystal structures of the same species (as they have not been determined), the calculated bond lengths are consistent with CH₃–Mg bond lengths (which range from 2.12 to 2.24 Å),^{36a} Mg–Cl bond lengths (which range from 2.27 to 2.53 Å),^{36a,b,d} and Mg–O bond lengths (which range from 1.90 to 2.71 Å for various O donor ligands)^{36a,b,d} determined for other organomagnesium species. Moreover, the differences of the coordination environments of these two structures is entirely consistent with (a) published

data on carboxylate ligands, which show that carboxylate anions can coordinate to magnesium in several ways including acting as bidentate ligands,³⁷ and (b) the fact that magnesium compounds show remarkably diverse coordination numbers, ranging from two through to eight and ten.³⁶

(b) Ion–Molecule Reactions of 1a and 1b. To evaluate whether the DFT-calculated differences in coordination at the magnesium center influence the bimolecular reactivity of these organomagnesates, **1a** and **1b** were mass-selected in MS³ experiments and allowed to react with a range of neutral reagents under the nearly thermal conditions of the ion trap.³⁸ Table 2 summarizes the results of these studies. Of the 14 neutral reagents examined (i.e., water, methanol, ethanol, five different aldehydes, acetic acid, acetone, methyl acetate, acetonitrile, trimethylborate, and methyl iodide), **1a** and **1b** only reacted with the first seven reagents via addition and methane expulsion (eq 13). These reactions are entirely consistent with the formulation of [CH₃MgL₂]⁻, as Grignard reagents are well known to react as bases in the condensed phase.³⁹ Moreover, this class of reaction also has precedence in the gas phase, with the tetramethyl aluminate anion undergoing similar reactions with acids (eq 14).⁴⁰



In an attempt to quantify these reactions, kinetic measurements were attempted for the reactive systems. Of the five reactive reagents, bimolecular rate constants were successfully determined from experiments for the reactions of **1a** and **1b** with (i) water, (ii) methanol, and (iii) ethanol. The reactions with the aldehydes proved to be too slow to measure, while acetic acid reacted with the organomagnesates at the collision rate.

Both organomagnesates react with water via addition and methane expulsion (eq 13, X = OH). Under identical conditions of water concentration and reaction time, **1a** (*m/z* 109, Figure S1c) reacts faster than **1b** (*m/z* 157, Figure S1f). This observation has been quantified by careful rate measurements (six independent measurements over several months): **1a** reacted at over

- (35) The B3LYP/6-31+G* level of theory predicts an activation energy of 71.2 kcal mol⁻¹ for the decarboxylation of CH₃CO₂H (data not shown), which is in good agreement with both the experimental estimates and previous theoretical calculations discussed above.³⁴ While we cannot comment on the absolute accuracy for the B3LYP/6-31+G*-predicted activation energies for the related decarboxylation reactions of the magnesium acetates, it is interesting to note that decarboxylation of CH₃CO₂H requires the highest activation energy, while the magnesium complexes appear to facilitate decarboxylation by lowering the activation barrier.
- (36) (a) Bickelhaupt, F. in *Grignard Reagents: New Developments*; Richey, H. G., Jr., Ed.; Wiley: Chichester, 2000; pp 299–328. (b) Uhm, H. L. In *Handbook of Grignard Reagents*; Silverman, G. S., Rakita, P. E., Eds.; Dekker: New York, 1996; pp 117–144. (c) Markies, P. R.; Akkerman, O. S.; Bickelhaupt, F.; Smeets, W. J. J.; Spek, A. L. *Adv. Organomet. Chem.* **1991**, *32*, 147. (d) Holloway, C. E.; Melnik, M. *Coord. Chem. Rev.* **1994**, *135/136*, 287. (e) Holloway, C. E.; Melnik, M. *J. Organomet. Chem.* **1994**, *465*, 1.
- (37) Deerfield, D. W., II; Fox, D. J.; Head-Gordon, M.; Hiskey, R. G.; Pedersen, L. G. *Proteins: Struct., Funct. Genet.* **1995**, *21*, 244.
- (38) Pioneering work by Gronert suggests that the ions in a modified LCQ ion trap mass spectrometer are essentially at room temperature, based upon equilibrium measurements [(a) Gronert, S. *J. Am. Soc. Mass Spectrom.* **1998**, *9*, 845] as well as kinetic measurements [(b) Flores, A. E.; Gronert, S. *J. Am. Chem. Soc.* **1999**, *121*, 2627].
- (39) For a review on Grignard reagents as bases, see: Kosar, W. In *Handbook of Grignard Reagents*; Silverman, G. S., Rakita, P. E., Eds.; Dekker: New York, 1996; Chapter 23.
- (40) Damrauer, R.; Krempp, M.; Damrauer, N. H.; Schmidt, M. W.; Gordon, M. S. *J. Am. Chem. Soc.* **1993**, *115*, 5218.

Table 2. Summary of the Ion–Molecule Reactions of $[\text{CH}_3\text{MgL}_2]^-$ with Various Neutral Reagents

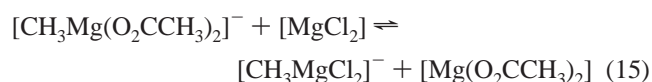
| reagent | gas-phase acidity, $\Delta_r H^\circ$, kcal mol ⁻¹ ^a | $[\text{CH}_3\text{MgCl}_2]^-$ | | | | $[\text{CH}_3\text{Mg}(\text{O}_2\text{CCH}_3)_2]^-$ | | | |
|---|---|---------------------------------|-------------------|----------|------------------|--|-------------------|----------|------------------|
| | | reaction (eqn no.) ^b | rate ^c | ϕ^d | ΔH° | reaction (eqn no.) ^b | rate ^c | ϕ^d | ΔH° |
| H ₂ O | 390.3 | 13 | 9.66 | 0.54 | -38.4 | 13 | 1.20 | 0.07 | -39.2 |
| CH ₃ OH | 382 | 13 | 8.71 | 0.57 | -39.0 | 13 | 1.31 | 0.09 | -40.6 |
| CH ₃ CH ₂ OH | 378.3 | 13 | 11.3 | 0.77 | | 13 | 1.47 | 0.11 | |
| CH ₃ C(O)H | 365.8 | 18 | <i>f</i> | | -33.9 | 18 | <i>f</i> | | -37.9 |
| EtC(O)H | 365.8 | 18 | <i>f</i> | | | 18 | <i>f</i> | | |
| PrC(O)H | 365.8 | 18 | <i>f</i> | | | 18 | <i>f</i> | | |
| CH ₃ CO ₂ H | 348.1 | 13 | <i>g</i> | | | 13 | <i>g</i> | | |
| PhC(O)H ^h | 369.1 | NR | | | | NR | | | |
| tBuC(O)H ^h | 369.1 | NR | | | | NR | | | |
| (CH ₃) ₂ CO | 369.1 | NR | | | | NR | | | |
| CH ₃ CO ₂ CH ₃ | 371.8 | NR | | | | NR | | | |
| CH ₃ CN | 372.9 | NR | | | | NR | | | |
| B(OCH ₃) ₃ | | NR | | | | NR | | | |
| CH ₃ I | 386.3 | NR | | | | NR | | | |

^a The gas-phase acidity of a molecule AH, $\Delta_{\text{acid}}H(\text{AH})$, is the enthalpy change at 298 K of the reaction: $\text{AH} \rightarrow \text{A}^- + \text{H}^+$ ^b Equation number refers to the equations in text. NR = no reaction. ^c Rate constants are in units of $10^{-10} \text{ cm}^3 \text{ molecule}^{-1} \text{ s}^{-1}$. Standard deviations in absolute rate constants were typically <10%. A conservative estimate of error is ± 25 , but relative rates are expected to be more accurate due to cancellation of errors. ^d Reaction efficiency: $\phi = k_{\text{exp}}/k_{\text{ADO}}$, where k_{ADO} is the theoretical prediction of the collision rate²⁶ between the $[\text{CH}_3\text{MgL}_2]^-$ (where L = Cl or O_2CCH_3) ion and a neutral base. ^e DFT-predicted reaction enthalpies in kcal mol⁻¹. For optimized structures and energetics, see Tables S1 and S2 and Figure S3 (Supporting Information). ^f Too slow to measure. ^g Reaction proceeds at collision rate. ^h Minor $[\text{RCO}_2\text{MgL}_2]^-$ products due to reaction with RCO_2H acid contaminants are observed.

50% of the collision rate (efficiency $\phi = 0.54$), while **1b** reacted only 7 out of every 100 collisions ($\phi = 0.07$) (Table 2).

When the organomagnesates **1a** and **1b** were subjected to similar experiments with methanol and ethanol, they were found to proceed via the same reaction pathway, i.e., addition of the ROH species (where R = CH₃ and CH₃CH₂), followed by methane expulsion (eq 13, X = OCH₃ and OCH₂CH₃) (Figure S4, Supporting Information). **1a** reacted at 50% and over of the collision rate with methanol and ethanol ($\phi = 0.57$ and $\phi = 0.77$, respectively), while **1b** reacted with methanol and ethanol at an efficiency of $\phi = 0.09$ and $\phi = 0.11$, respectively. Thus, in both instances **1a** and **1b** were found to react most efficiently with ethanol, followed by methanol and then water, which follows the gas-phase acidity order of HX.⁴¹ More importantly, all kinetic studies support an enhanced reactivity of **1a** over **1b** and demonstrate a clear example of how the ancillary ligands (L) can effect the reactivity of organomagnesates.

To gain insights into the nature of these novel ligand effects, we have carried out DFT calculations on the full reaction coordinates for **1a** and **1b** reacting with water (Figures 3 and S3). These reactions follow the classical Brauman “double-well” reaction coordinate by exhibiting the formation of pre- and postreaction complexes.⁴² A noteworthy aspect of these DFT calculations is that higher reactivity of **1a** toward H₂O cannot be explained by the thermodynamics. Not only are the overall reaction enthalpies predicted to be more exothermic for **1b**, but the relative methyl anion affinities of MgCl_2 and $\text{Mg}(\text{O}_2\text{CCH}_3)_2$, as predicted by eq 15, reveal that **1b** should be the better methyl anion donor.⁴³ Furthermore, electrostatics cannot be used to



explain the difference in the reactivity since **1b** is predicted to have a higher positive charge at the magnesium atom (Mulliken charges are **1a** Mg +0.72; **1b** Mg +1.12). Figure 3 reveals that the activation energy (the difference in energy between the

pre-reaction complexes and the transition states) accounts for the observed reactivity trends, with **1a** experiencing an activation energy of 2.8 kcal mol⁻¹ relative to 7.2 kcal mol⁻¹ for and **1b**. The DFT calculations also provide unique structural insights, revealing that lower coordination around the magnesium center of **1a** is at the heart of its enhanced reactivity (Figure S3). Thus **1a** is tricoordinate, while all of the acetate ligands in **1b** act as bidentate ligands, making the magnesium atom five-coordinate.³⁷ Both **1a** and **1b** form transition states (Figure 3a,b), in which the incoming water becomes coordinated (Figure S3). Thus, **1b** suffers from overcrowding of its coordination sphere in the transition state relative to that of **1a**.^{36,44} While steric effects of the alkyl group are known to influence the reactivity of Grignard reagents in the condensed phase,⁴⁵ this gas-phase study provides some of the first mechanistic insights into how the ancillary ligand can change the coordination environment around the magnesium atom and thereby influence the reactivity of Grignard reagents.⁴⁶

Similar DFT calculations were also carried out for the $[\text{CH}_3\text{MgCl}_2]^-$ species reacting with methanol. The structures and reaction coordinate are shown in Supplementary Figures S5. As in the previous case, **1a** is tricoordinate species that forms a transition state in which the incoming methanol becomes coordinated. This is then followed by methane expulsion.

(41) <http://webbook.nist.gov/chemistry/>

(42) Brauman, J. I. *J. Mass Spectrom.* **1995**, *30*, 1649.

(43) Surprisingly, no gas-phase thermodynamic methyl anion affinity scale for neutrals exists. For a hydride ion affinity scale, see: Squires, R. R. In *Structure/Reactivity and Thermochemistry of Ions*; Ausloos, P., Lias, S. G., Eds.; Reidel: Dordrecht, 1987; pp 373–375.

(44) This represents a rare example of how differences in coordination can influence the gas-phase reactivity of an organometallic species. For some key references on other types of ligand effects in the gas-phase ion–molecule reactions of metal complexes, see: (a) Tjelja, B. L.; Armentrout, P. B. *J. Am. Chem. Soc.* **1996**, *118*, 9652. (b) Schröder, D.; Schwarz, H. J. *Organomet. Chem.* **1995**, *504*, 123. (c) Richardson, D. E.; Alameddini, N. G.; Ryan, M. F.; Hayes, T.; Eyley, J. R.; Siedle, A. R. *J. Am. Chem. Soc.* **1996**, *118*, 11244.

(45) Yang, K.-C.; Chang, C.-C.; Yeh, C.-S.; Lee, G.-H.; Peng, S.-M. *Organometallics* **2001**, *20*, 126.

(46) It is interesting to note that there has been a condensed phase report on the enhanced selectivity (i.e., reduced reactivity) of Grignard reagents processing carboxylate ligands instead of the traditional halides: Reetz, M. T.; Harmat, N.; Mahrwald, R. *Angew. Chem., Int. Ed. Engl.* **1992**, *31*, 342.

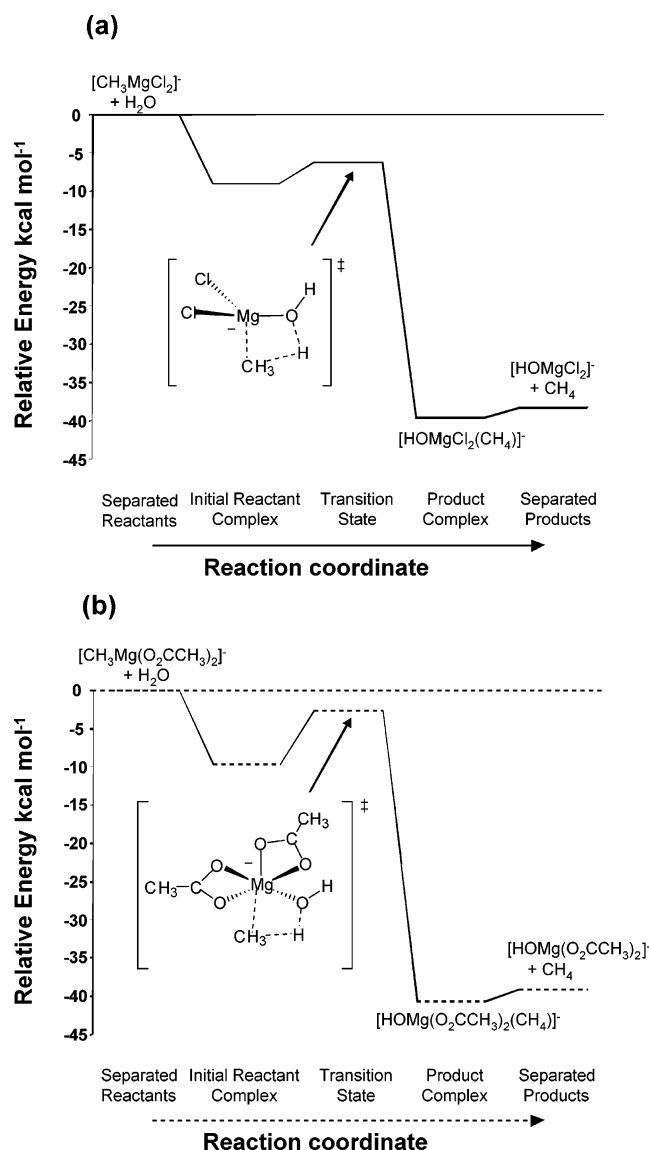


Figure 3. Plot of B3LYP/6-31+G*—calculated reaction coordinate for ion–molecule reactions of (a) $[\text{CH}_3\text{MgCl}_2]^-$ with H_2O and (b) $[\text{CH}_3\text{Mg}(\text{O}_2\text{CCH}_3)_2]^-$ with H_2O .

Examination of the difference between the pre complex and the transition state reveals an activation energy of $3.9 \text{ kcal mol}^{-1}$ for this system (cf. $2.8 \text{ kcal mol}^{-1}$ for the water system). Note however, that the overall barrier for the methanol system is slightly lower (i.e. $-6.4 \text{ kcal mol}^{-1}$ relative to separated reactants, Figure S5) than that of the water system (i.e. $-6.3 \text{ kcal mol}^{-1}$ relative to separated reactants, Figure 3). This is entirely consistent with our experimental data which shows that **1a** reacts with methanol only slightly more efficiently (i.e. $\phi=0.57$) than with water (i.e. $\phi=0.54$).

(c) Ion–Molecule Reactions with Aldehydes. The reactions of anions with carbonyl compounds have been extensively studied in the gas phase.^{16a,47a–d} Simple aldehydes with enolizable hydrogens often undergo competition between enolization (deprotonation) and addition. Both reaction channels are predicted to be highly exothermic for the bare methyl anion reacting with acetaldehyde ($-49.8 \text{ kcal mol}^{-1}$ for enolization and $-48.2 \text{ kcal mol}^{-1}$ for addition).⁴⁰ Indeed, Graul and Squires observed both reactions for the bare methyl anion reacting with propionaldehyde (eqs 16 and 17), with the highly exothermic

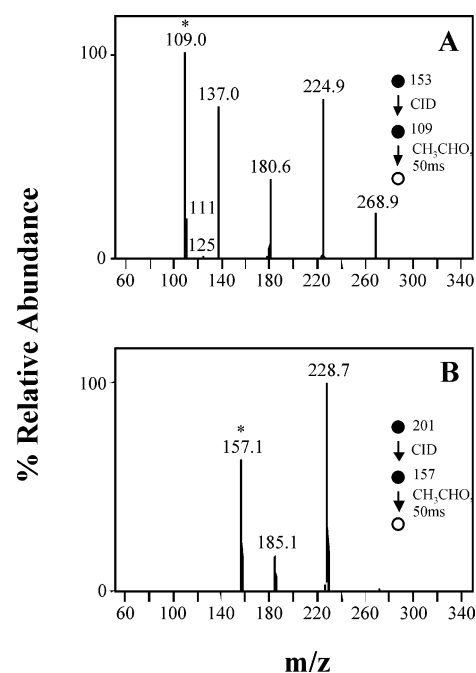


Figure 4. Multistage mass spectrometry experiments for the ion–molecule reactions between acetaldehyde and the mass-selected organomagnesates: (a) $[\text{CH}_3^{24}\text{Mg}^{35}\text{Cl}_2]^-$ (m/z 109) and (b) $[\text{CH}_3^{24}\text{Mg}(\text{O}_2\text{CCH}_3)_2]^-$ (m/z 157). The product ions for $[\text{CH}_3^{24}\text{Mg}^{35}\text{Cl}_2]^-$ (m/z 109) correspond to $[\text{CH}_2\text{CHO}^{24}\text{Mg}^{35}\text{Cl}_2]^-$ (m/z 137) with subsequent additions of one, two, and three acetaldehydes (m/z 181, 225, 269), respectively. The product ions for $[\text{CH}_3^{24}\text{Mg}(\text{O}_2\text{CCH}_3)_2]^-$ (m/z 157) correspond to $[\text{CH}_2\text{CHO}^{24}\text{Mg}(\text{O}_2\text{CCH}_3)_2]^-$ (m/z 185) with subsequent addition of one acetaldehyde (m/z 229).

addition reaction leading to fragmentation (eq 17).¹⁷ To determine how coordination of CH_3^- to MgL_2 influences its reactivity toward aldehydes,^{47e} we have used a combination of experiments on the reactions of **1a** and **1b** with five aldehydes (Table 2 and Figure 4) and DFT calculations on the acetaldehyde system (Tables S1–S3 and Figure S3).

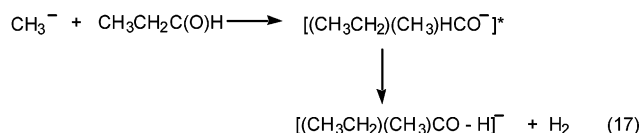
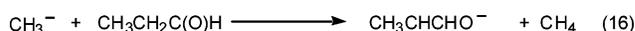
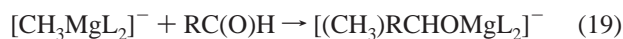
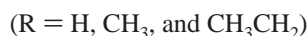
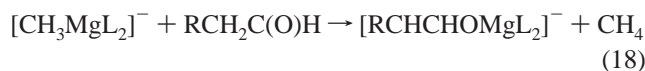


Figure 4 shows that **1a** (i.e., $[\text{CH}_3\text{MgCl}_2]^-$ (m/z 109)) reacts with acetaldehyde via addition and then loss of CH_4 to form the enol product $[\text{CH}_2\text{CHOMgCl}_2]^-$ (m/z 137) (eq 18). This is followed by three subsequent additions of acetaldehyde (m/z 181, +1 CH_3CHO ; m/z 225, +2 CH_3CHO ; m/z 269, +3 CH_3CHO) (Figure 4a). While **1b** (i.e., $[\text{CH}_3\text{Mg}(\text{O}_2\text{CCH}_3)_2]^-$ (m/z 157)) reacts similarly with acetaldehyde to initially form the enol product $[\text{CH}_2\text{CHOMg}(\text{O}_2\text{CCH}_3)_2]^-$ (m/z 185) (eq 18), the enol product undergoes only one subsequent addition of acetaldehyde (i.e., m/z 229, +1 CH_3CHO) (Figure 4b). Perhaps the most noteworthy aspect of the reactions of **1a** and **1b** with

(47) For a review, see: (a) Riveros, J. M.; Jose, S. M.; Takashima, K. *Adv. Phys. Org. Chem.* **1985**, *21*, 197. For examples of gas-phase C–C bond-forming reactions between carbonyl compounds and bare carbanions, see: (b) Bartmess, J. E.; Hays, R. L.; Caldwell, G. *J. Am. Chem. Soc.* **1981**, *103*, 1338. (c) Hayes, R. N.; Grese, R. P.; Gross, M. L. *J. Am. Chem. Soc.* **1989**, *111*, 8336. (d) Hass, G. W.; Gross, M. L. *J. Am. Soc. Mass Spectrom.* **1996**, *7*, 82. Aldehydes are more reactive than ketones in nucleophilic reactions; see: (e) Smith, M. B.; March, J. *March's Advanced Organic Chemistry*, 5th ed.; Wiley: New York, 2001; pp 1172–1175.

CH₃CHO is that the Grignard reactions do not occur (eq 19). The reactions of propionaldehyde and butyraldehyde (Table 2) also solely proceed via enolization (eq 18). In fact, when the possibility of enolization is thwarted, the Grignard reaction still fails to proceed (eq 19), as exemplified when **1a** and **1b** are exposed to benzaldehyde and pivaldehyde (Table 2).



The competition between enolization and the Grignard reaction is not without precedence. In fact, Grignard reagents with larger alkyl groups possessing β H atoms can undergo an additional competing reaction in which the Grignard reagent acts as a reducing agent.⁴⁸ These three competing reactions reflect the different characteristics of Grignard reagents (base versus nucleophile versus reductant) and carbonyl compounds (acid versus electrophile versus oxidant) and occur by different mechanisms.⁴⁹ In the enolization reaction, the Grignard reagent acts as a base³⁹ and deprotonates the carbonyl compound to yield the magnesium enolate product. While at first glance it may seem surprising that the enol reaction (eq 18) can dominate over the Grignard reaction (eq 19), Han and Parkin have shown that the monomeric organomagnesium compound, **2**, can react with a small (i.e., non-sterically hindered) ketone such as acetone solely via the enolization pathway.⁵⁰ A more recent study on a related monomeric organomagnesium compound, **3**, also showed the domination of the enolization channel and provided an X-ray crystal structure of the magnesium enolate product.⁵¹

To gain further mechanistic insights into why the enolization reaction (eq 18) occurs in preference to the Grignard reaction (eq 19) in the gas phase, we have carried out DFT calculations on the reaction coordinates for **1a** and **1b** reacting with acetaldehyde. Figure 5 illustrates the reaction coordinates of the $[\text{CH}_3\text{MgL}_2]^-$ species (when L = Cl and O₂CCH₃, respectively) reacting with acetaldehyde (structures of all species are shown in Figure S3). Both **1a** and **1b** react with acetaldehyde via distorted double-well surfaces involving the initial formation of two reactant complexes: (i) the precomplex for the enol reaction (Figure 5a for **1a** and Figure 5c for **1b**) and (ii) the precomplex for the Grignard reaction (Figure 5b for **1a** and Figure 5d for **1b**). It is worth noting that condensed-phase studies also point to the formation of precomplexes in which the carbonyl compound initially binds to the magnesium center for both the enolization reaction^{52a} and the Grignard reaction.^{52b} Furthermore, DFT^{14a} and ab initio^{14c,d} calculations on other models for Grignard reactions of carbonyl compounds also show the formation of a precomplex. An examination of the structures

of the B3LYP/6-31+G*-calculated complexes (Figure S3) reveals some interesting differences. The enol and Grignard precomplexes for **1a** have similar energies (Figure 5a,b) and structures in which a tetrahedral complex is formed by coordinating the oxygen of acetaldehyde to the magnesium center. In contrast, the precomplexes for **1b** reacting with CH₃CHO have slightly different energies (Figure 5c,d) and involve structures in which CH₃CHO forms weakly bound hydrogen-bonded complexes with the acetate ligands of **1b**. Despite the differences in the structures of the precomplexes, the DFT calculated transition-state structures are consistent with previous mechanistic discussions on the Grignard and enolization reactions.⁴⁹ Thus, six-centered transition states are observed for the enolization reactions (Figure 5a,c), while the Grignard reactions can be regarded as proceeding via four-centered transition states (Figure 5b,c).

Turning our attention to energetics associated with the reaction coordinates (Figure 5), we notice that both the enolization and Grignard reactions are predicted to have barrier heights which are above the total energy of the separated reactants. While this suggests that the B3LYP/6-31+G* level of theory underestimates the energies of the transition states,³⁰ it is worth recalling that the actual experimentally observed reaction (eq 18) is slow. Perhaps a greater surprise is that the Grignard reaction (eq 19) is theoretically predicted to be favored over the enolization reaction (eq 18) on thermodynamic grounds. Thus, the barrier height for the Grignard reaction is slightly lower for both **1a** and **1b**, while the energetics associated with the formation of the coordinated Grignard product, $[(\text{CH}_3)_2\text{CHOMgL}_2]^-$, is favored. Furthermore, these two competing processes have quite different outcomes in terms of the initial products (i.e., post-transition-state complexes) formed. Whereas the enol product is a weakly bound ion–molecule complex between $[\text{CH}_2\text{CHOMgL}_2]^-$ and methane which can readily expel methane to give the observed magnesium enolate, $[\text{CH}_2\text{CHOMgL}_2]^-$, the initially formed Grignard product is the coordinated alkoxide, $[(\text{CH}_3)_2\text{CHOMgL}_2]^-$. Previous DFT^{14a} and ab initio^{14c,d} calculations on other models for Grignard reactions of carbonyl compounds also show the formation of magnesium alkoxides in highly exothermic reactions. While this Grignard product is formed with an excess energy (approximately 40 kcal mol⁻¹ in Figure 5b,d), the exoothermicity is not large enough to drive fragmentation to the bare alkoxide ion, $(\text{CH}_3)_2\text{CHO}^-$, and MgL₂ (eq 20, Figure 5b,d).



How can these theoretical results be reconciled with the experimental observation that the enol product (eq 18) is solely observed? A likely explanation is that the Grignard reaction (eq 19) suffers more from entropic factors than the enolization reaction (eq 18).⁵³ To test this hypothesis, we have carried out a simplified analysis of the Arrhenius factors for the two competing reactions in the case of $[\text{CH}_3\text{MgCl}_2]^-$ reacting with acetaldehyde. This system was chosen since the enol and

(48) Cowan, D. O.; Mosher, H. S. *J. Org. Chem.* **1962**, *27*, 1.

(49) For a recent discussion on the mechanisms of these competing reactions, see: Holm, T.; Crossland, I. In *Grignard Reagents: New Developments*; Richey, H. G., Jr., Ed.; Wiley: Chichester, 2000; Chapter 1.

(50) Han, R.; Parkin, G. *J. Am. Chem. Soc.* **1992**, *114*, 748.

(51) Dove, A. P.; Gibson, V. C.; Marshall, E. L.; White, A. J. P.; Williams, D. *J. Chem. Commun.* **2002**, 1208.

(52) (a) Pinkus, A. G.; Sabesab, A. *J. Chem. Soc., Perkin Trans. 2* **1981**, 473. (b) Ashby, E. C.; Laemmle, J.; Neumann, H. M. *Acc. Chem. Res.* **1974**, *7*, 272.

(53) An alternative explanation that the Grignard reaction is reversible seems less likely. This is due to the fact that, although the energized Grignard products are expected to be able to dissipate their energy more readily for the larger aldehydes, no such reaction is observed. For examples of reversible Grignard reactions in the condensed phase, see: (a) Benkeser, R. A.; Siklosi, M. P.; Mozdzen, E. C. *J. Am. Chem. Soc.* **1978**, *100*, 2134. (b) Benkeser, R. A.; Siklosi, M. P. *J. Org. Chem.* **1976**, *41*, 3212.

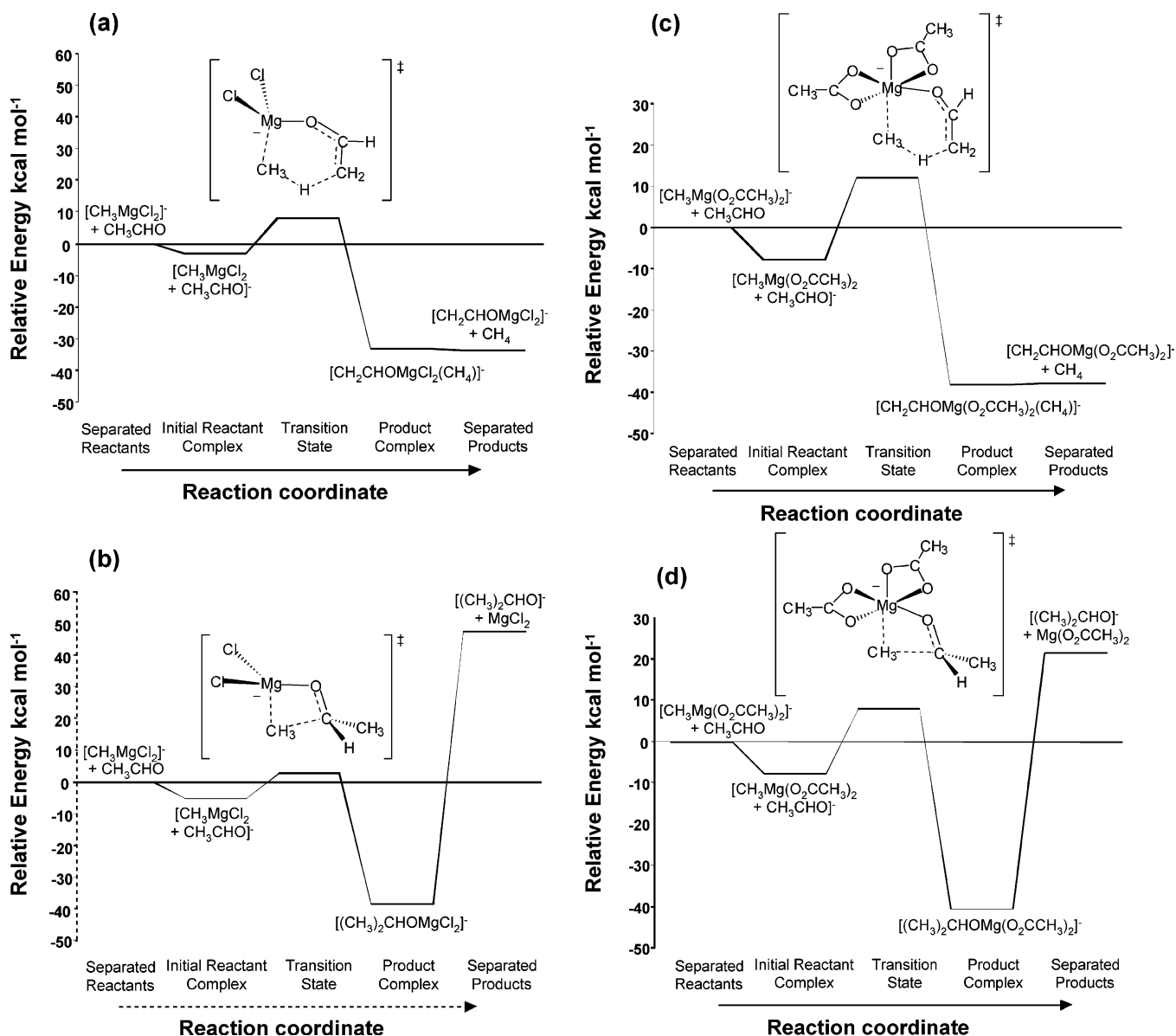


Figure 5. Plot of B3LYP/6-31+G*⁻-calculated reaction coordinates for ion–molecule reactions of CH₃CHO with (a) [CH₃MgCl₂]⁻ via the enolization reaction (eq 18); (b) [CH₃MgCl₂]⁻ via the Grignard reaction (eqs 19 and 20); (c) [CH₃Mg(O₂CCH₃)₂]⁻ via the enolization reaction (eq 18); and (d) [CH₃Mg(O₂CCH₃)₂]⁻ via the Grignard reaction (eqs 19 and 20).

Grignard precomplexes have similar energies and structures, allowing us to use the DFT-calculated vibrational frequencies for each transition state to estimate their vibrational partition functions ($Q_{\text{vib}}^{\ddagger}$), as detailed by Bowie's group.⁵⁴ Such an analysis reveals that the enol transition state has a $Q_{\text{vib}}^{\ddagger}$ nearly 3 times larger than that for the Grignard transition state, suggesting it is "looser" (Table S3). Thus, the Grignard transition state appears to suffer entropically relative to the enol transition state, nicely reconciling the experimental and theoretical results.

Returning to Figure 4, it is interesting to note that, while both [CH₃MgL₂]⁻ species result in enolization product ions, the enolate [CH₂CHOMgL₂]⁻ undergoes subsequent additions of up to three acetaldehydes, while [CH₂CHOMg(O₂CCH₃)₂]⁻ only adds one. Mass selection of [CH₂CHOMgL₂]⁻ confirms that

each CH₃CHO adds in a stepwise fashion (data not shown). What possible structures could account for the further addition of CH₃CHO to the magnesium enolates, [CH₂CHOMgL₂]⁻? An examination of the condensed phase literature reveals two possible scenarios for the interaction of magnesium enolates⁵⁵ with carbonyl compounds: (a) simple solvation of the Mg center^{55c} and (b) an aldol reaction between the coordinated enolate and a neutral acetaldehyde.^{56,57} An example of the former case involves a magnesium bisenolate terminated by solvating ketone, which can be considered as a model, aggregated, pre-aldol intermediate.^{55c} In either scenario, if all the acetaldehyde molecules end up coordinating to the magnesium centers, then both of the resultant complexes [CH₂CHOMgCl₂ + 3CH₃CHO]⁻ and [CH₂CHOMg(O₂CCH₃)₂ + CH₃CHO]⁻ end up with a coordination number of 6. It is worth noting that, while magnesium compounds can show remarkably diverse coordination numbers, the preferred coordination number for divalent magnesium is 6.^{36a}

(54) For a detailed discussion of the underlying assumptions of this approach and examples in gas-phase anion chemistry, see: (a) Hevko, J. M.; Dua, S.; Bowie, J. H.; Taylor, M. S. *J. Chem. Soc., Perkin Trans. 2* **1999**, 457. (b) McAnoy, A. M.; Dua, S.; Balnksby, S. J.; Bowie, J. H. *J. Chem. Soc., Perkin Trans. 2* **2000**, 1665.

To gain insights into these competing processes, DFT calculations were carried out on the “solvated” enol versus aldol products for structures containing the maximum number of coordinated CH_3CHO . Figure S3 shows the structures of the “solvated” enol ($[\text{CH}_2\text{CHOMgL}_2]^- + n\text{CH}_3\text{CHO}$) species (where $L = \text{Cl}$ and $n = 3$; and $L = \text{CH}_3\text{CO}_2$ and $n = 1$) and reveals that the $[\text{CH}_2\text{CHOMgCl}_2]^-$ complex is capable of accommodating more acetaldehyde species than its $[\text{CH}_2\text{CHOMg}(\text{O}_2\text{CCH}_3)_2]^-$ counterpart, which correlates with our experimental data. This is predominately due to the fact that the CH_3CO_2 ligands in $[\text{CH}_2\text{CHOMg}(\text{O}_2\text{CCH}_3)_2]^-$ bind to the magnesium in a bidentate fashion, thereby precluding the binding of two more acetaldehyde ligands. In both cases, the coordination number at the magnesium center is 6.

It is interesting to compare the “solvated” enol product ions to their isomeric aldol structures (Figure S3). In the case of the “solvated” enol product ions, the enolate and neutral acetaldehyde were separate entities that were bound to magnesium through their oxygen atoms. In the case of the aldol product ions, however, the enolate and neutral acetaldehyde react via C–C bond formation to produce the new ligand, $\text{HC}(\text{O})\text{CH}_2\text{CH}(\text{O}^-)\text{CH}_3$, which binds in a bidentate fashion (through both oxygen atoms) to Mg. While we cannot prove the actual structure of the experimentally observed products, it is worth noting that in all cases, the coordination number at the magnesium center is 6, consistent with the observed number of acetaldehyde molecules added. On energetic grounds (Tables S1 and S2), the DFT calculations suggest that the aldol species may be formed since the solvation by only one acetaldehyde of the enol $[\text{CH}_2\text{CHOMg}(\text{O}_2\text{CCH}_3)_2]^-$ is predicted to exothermic by $0.7 \text{ kcal mol}^{-1}$, while the aldol product is predicted to exothermic by 5 kcal mol^{-1} . A similar situation holds for the enol $[\text{CH}_2\text{CHOMgCl}_2]^-$, for which solvation by three acetaldehydes is predicted to be exothermic by $6.8 \text{ kcal mol}^{-1}$ while formation of the aldol plus solvation by the remaining two acetaldehydes is predicted to be exothermic by $9.2 \text{ kcal mol}^{-1}$. Overall these results are intriguing since, while the Grignard reaction fails, addition of acetaldehyde to the magnesium enolates (products of eq 18) readily occurs. Unfortunately, a detailed DFT search of the reaction coordinate for the “aldol reactions” is beyond our computational resources, but a simple consideration of the ring sizes of the transition states for the Grignard (four-centered) versus aldol (six-centered) reactions suggests that the latter may be more favored.

(d) A Novel Catalytic Cycle for the Decarboxylation of Acetic Acid. The thermal decomposition of acetic acid is of considerable interest.³⁴ In the absence of catalyst, two competing sets of products are formed: (i) ketene and water, and (ii) methane and carbon dioxide. The former products are formed about twice as much as the latter.^{34d} We have recently used multistage mass spectrometry experiments to show that metal catalysts can favor the selective dehydration of acetic acid to ketene via a two-step gas-phase catalytic cycle (Figure 6a).³³ The catalysts were Group VI mononuclear $[\text{Mo}_3(\text{OH})]^-$ and binuclear $[\text{M}_2\text{O}_6(\text{OH})]^-$ oxo-anions ($M = \text{Mo}, \text{W}$).

In the present work, the observation of two key steps—(a) decarboxylation of a magnesium acetate, $[\text{CH}_3\text{CO}_2\text{MgL}_2]^-$, to form a Grignard, $[\text{CH}_3\text{MgL}_2]^-$ (eq 10), and (b) reaction of the resultant Grignard, $[\text{CH}_3\text{MgL}_2]^-$, with acetic acid to re-form the magnesium acetate, $[\text{CH}_3\text{CO}_2\text{MgL}_2]^-$ (eq 13, where $X =$

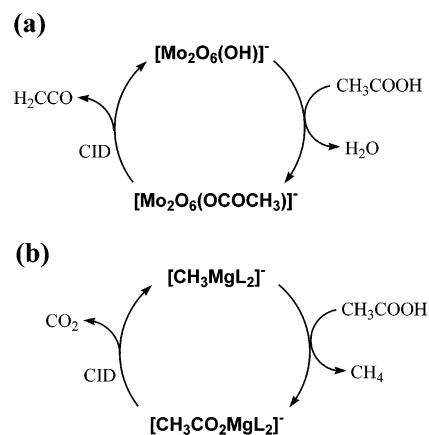


Figure 6. Gas-phase catalytic cycles for (a) the dehydration of acetic acid and (b) the decarboxylation of acetic acid.

CH_3CO_2)—suggests a simple two-step catalytic cycle for the decomposition of acetic acid into methane and carbon dioxide (Figure 6b). Although both of these reactions have been discussed in previous sections, it is worth recalling several points: (i) the rate-determining step is the decarboxylation reaction (eq 10); (ii) $[\text{CH}_3\text{CO}_2\text{MgCl}_2]^-$ is expected to be a better catalyst since not only does it have a lower activation energy, but it does not suffer from the alternative acetate loss channel (eq 11); and (iii) although the crude estimate of $64 \pm 20 \text{ kcal mol}^{-1}$ determined here for the critical energy of CO_2 elimination from $[\text{CH}_3\text{CO}_2\text{MgCl}_2]^-$ is very close to the estimated activation energy (in the range of $67\text{--}72 \text{ kcal mol}^{-1}$)³⁴ for decarboxylation of acetic acid, the DFT calculations suggest that the decarboxylation reactions should be regarded as catalytic since the B3LYP/6-31+G*-calculated activation energies are less than that for acetic acid.³⁵

Using the multistage trapping capabilities of the ion trap instrument, it was possible to establish the cycle as truly catalytic by carrying out the two reactions two times on the same population of starting ions (data not shown). Note that due to the loss of signal, the maximum number of turns (six times) through the catalytic cycle possible for our instrument (i.e., an MS^{10} experiment) could not be achieved. By monitoring the reduction in intensity of the catalytic ion $[\text{CH}_3\text{MgCl}_2]^-$, it was possible to approximate the amount of the ion lost through each complete catalytic cycle. The CID step is the least efficient, with only about 15–20% of the parent signal of $[\text{CH}_3\text{CO}_2\text{MgCl}_2]^-$ being converted to mass-selected $[\text{CH}_3\text{MgCl}_2]^-$ ions ready for the next step. We have previously noted that some small metal ions undergo loss of signal under CID conditions.³³ While a possible explanation is collision-induced electron loss, a more likely explanation is the poor trapping efficiency of smaller CID products formed in the ion trap. As the mass-selected $[\text{CH}_3\text{MgCl}_2]^-$ ions react with acetic acid (see Figure S6, Supporting Information) at the collision rate, this reaction is the most efficient in the ion trap. Nonetheless, since it is impossible to exclude the background ESI solvents (water and methanol), at best only about 65% of the mass-selected $[\text{CH}_3\text{MgCl}_2]^-$ ions are converted to mass-selected $[\text{CH}_3\text{CO}_2\text{MgCl}_2]^-$ ions for the next catalytic cycle. These experiments suggest that slightly less than 10% of the catalytic ion $[\text{CH}_3\text{MgCl}_2]^-$ can be “recovered” across the two reactions of a single catalytic cycle. Given that ions are expected to be lost from the ion trap in our experiments, and that ions are also lost

due to incomplete reactions, this estimate represents an absolute lower bound on the efficiency of this process.

Our observation of a catalytic cycle for the decomposition of acetic acid which is catalyzed by an organometallic intermediate prompted the question, are such processes known in the condensed phase? While there have been several reports on the use of copper(I) salts to catalyze the decomposition of carboxylic acids, work by Darensbourg suggest that the mechanisms of these catalytic reactions are quite complex and may not involve an organometallic intermediate, but rather involve electrophilic intermediates.⁵⁸ Thus, the gas-phase cycle shown in Figure 6b appears to be a unique example of the involvement of an organometallic intermediate in the decomposition of a carboxylic acid.

Conclusions

Decarboxylation of acetate complexes $[\text{CH}_3\text{CO}_2\text{MgL}_2]^-$ (where $\text{L} = \text{Cl}$ and O_2CCH_3) resulted in the gas-phase synthesis of the organomagnesates $[\text{CH}_3\text{MgL}_2]^-$. Using established critical energies for the dissociation of $\text{Ag}(\text{CH}_3\text{OH})^+$ and $\text{Fe}(\text{C}_5\text{H}_5)_2^+$, we were able to “bracket” the activation voltages for these decarboxylation reactions at 0.70 and 0.78 $\text{V}_{\text{p-p}}$ for $[\text{CH}_3\text{CO}_2\text{MgCl}_2]^-$ and $[\text{CH}_3\text{CO}_2\text{Mg}(\text{O}_2\text{CCH}_3)_2]^-$, respectively. While exclusive decarboxylation occurred upon CID of the $[\text{CH}_3\text{CO}_2\text{MgCl}_2]^-$ complex, $[\text{CH}_3\text{CO}_2\text{Mg}(\text{O}_2\text{CCH}_3)_2]^-$ fragments via competing acetate ion formation and decarboxylation, with the former dominating. DFT calculations on the reaction coordinates associated with decarboxylation revealed a different reactant geometry for $[\text{Mg}(\text{O}_2\text{CCH}_3)_3]^-$ but not for $[\text{CH}_3\text{CO}_2\text{MgCl}_2]^-$. The bimolecular reactivity of the organomagnesates **1a** and **1b** was examined via ion–molecule reactions with a number of neutral reagents. Both organomagnesates were able to react with water, methanol, and ethanol via addition and methane expulsion (eq 13) in the order ethanol (most efficient) > methanol > water (least efficient). Overall, the $[\text{CH}_3\text{MgCl}_2]^-$ complexes were observed to react faster with the neutral reagents compared with the $[\text{CH}_3\text{Mg}(\text{O}_2\text{CCH}_3)_2]^-$ species. DFT calculations on the water reactions reveal that lower coordination around the magnesium center of **1a** is at the heart of its enhanced reactivity. Ion–molecule reactions with acetaldehyde yielded some interesting observations. Rather than forming an adduct species (i.e., the

Grignard reaction), **1a** and **1b** reacted to form the magnesium enolates $[\text{CH}_2\text{CHOMgL}_2]^-$. A simplified Arrhenius analysis of the DFT calculated reaction coordinates for these competing reactions for **1a** suggest that while the Grignard reaction is enthalpically favored, it suffers entropically. It is interesting to compare the acid–base reactions of $[\text{CH}_3\text{MgCl}_2]^-$ complexes with different types of acids (eq 13). Although acetaldehyde is much more acidic than water (nearly 25 kcal mol^{-1} , Table 2), it undergoes this reaction much less readily with **1a** and **1b**. This illustrates a dramatic impact of metal coordination on the effective acidity of the reagent, further confirmed by the DFT-calculated energetics (Table S2), which suggest kinetic barriers as well as a thermodynamic effect (the overall enthalpy changes of the water and acetaldehyde reactions are essentially the same).

Finally, a two-step gas-phase catalytic cycle is presented for the decarboxylation of acetic acid using the $[\text{CH}_3\text{MgL}_2]^-$ species (when $\text{L} = \text{Cl}$, O_2CCH_3) (Figure 6b). The first step involves addition of $\text{CH}_3\text{CO}_2\text{H}$ with elimination of CH_4 to yield $[\text{CH}_3\text{CO}_2\text{MgL}_2]^-$. The second step involves decarboxylation under conditions of collisional activation to yield the $[\text{CH}_3\text{MgL}_2]^-$ species. Further work is underway to study the formation and reactions of other organometallic ions.

Acknowledgment. This paper is dedicated to Professor Michael Bruce, FRS, on the occasion of his 65th birthday and in recognition of his many important contributions to organometallic and cluster chemistry. This work is supported by the Australian Research Council. We thank (i) the Melbourne Advanced Research Computing Centre (MARCC) for their generous allocation of computer time; (ii) Professor John Bowie and Dr. Andrew McAnoy for helpful discussion on the calculation of Arrhenius factors; and (iii) Mr. David McNaught for carrying out some preliminary experiments. A.K.V. acknowledges the award of a Science Faculty Scholarship (Studentship). We thank Mr. Tom Waters for useful discussions on the decomposition of acetic acid and the measurements of threshold dissociation energies.

Supporting Information Available: CID mass spectra of the organomagnesates reagents and their ion–molecule reactions with water; branching ratio measurements for CID of $[\text{CH}_3\text{CO}_2\text{Mg}(\text{O}_2\text{CCH}_3)_2]^-$; structures and coordinates of all species calculated for the reactions shown in Figures 2, 3, and 5, and S5; mass spectra of the ion–molecule reactions between the organomagnesates and methanol and ethanol; plot of B3LYP/6-31+G*-calculated reaction coordinate for ion–molecule reactions of $[\text{CH}_3\text{MgCl}_2]^-$ with CH_3OH ; mass spectra of the ion–molecule reactions between the organomagnesates and acetic acid; DFT energies of all species used to calculate thermochemistry; DFT-calculated thermochemistry (at the B3LYP/6-31+G* + 0.9806 ZPVE level of theory); pre-exponential Arrhenius factors for competing reactions of $[\text{CH}_3\text{MgCl}_2]^- + \text{CH}_3\text{CHO}$. This material is available free of charge via the Internet at <http://pubs.acs.org>.

JA048476W

- (55) Magnesium enolates can be formed via a range of processes, and several have been characterized by X-ray crystallography: (a) Willard, P. G.; Salvino, J. M. *Chem. Commun.* **1986**, 153. (b) Allan, J. F.; Clegg, W.; Henderson, K. W.; Horsburgh, L.; Kennedy, A. R. *J. Organomet. Chem.* **1998**, 559, 173. (c) Allan, J. F.; Henderson, K. W.; Kennedy, A. R.; Teat, S. J. *Chem. Commun.* **2000**, 1059.
- (56) The aldol reaction is an important way of forming C–C bonds. For an overview, see: (a) Smith, M. B.; March, J. *March's Advanced Organic Chemistry*, 5th ed.; Wiley: New York, 2001; pp 1218–1223. For a recent X-ray crystal structure of a magnesium adolate, see: (b) Allan, J. F.; Henderson, K. W.; Kennedy, A. R. *Chem. Commun.* **1999**, 1325.
- (57) For recent studies on the gas-phase fragmentation reactions of aldol complexes of metals, see: Shvartsburg, A. A.; Wilkes, J. G. *Int. J. Mass Spectrom.* **2003**, 225, 155.
- (58) (a) Darensbourg, D. J.; Holtcamp, M. W.; Longridge, E. M.; Khandelwal, B.; Klausmeyer, K. K.; Reibenspies, J. H. *J. Am. Chem. Soc.* **1995**, 117, 318. (b) Darensbourg, D. J.; Holtcamp, M. W.; Khandelwal, B.; Klausmeyer, K. K.; Reibenspies, J. H. *Inorg. Chem.* **1995**, 34, 2389.